

1     **PREDICTING LIFT-OFF TIME WHEN DEEP-FRYING POTATO**  
2                             **DOUGH SNACKS** \*

3     T. BABB, <sup>†</sup>, G.P. BENHAM <sup>‡</sup>, J. BOWS <sup>§</sup>, R. GONZALEZ-FARINA<sup>†</sup>, K. B. KIRADJIEV<sup>†</sup>  
4                             , W. T. LEE <sup>¶</sup>, AND S. TIBOS <sup>§</sup>

5     **Abstract.** When frying potato snacks, it is typically observed that the dough, which is sub-  
6 merged in hot oil, after some critical time increases its buoyancy and floats to the surface. The  
7 lift-off time is a useful metric in ensuring that the snacks are properly cooked. Here we propose  
8 a multiphase mathematical model for the frying of potato snacks, where water inside the dough is  
9 evaporated from both the top and bottom surfaces of the snack at two receding evaporation fronts.  
10 The vapour created at the top of the snack bubbles away to the surface, whereas the vapour released  
11 from the bottom surface forms a buoyant blanket layer. By asymptotic analysis, we show that the  
12 model simplifies to solving a one-dimensional Stefan problem in the snack coupled to a thin-film  
13 equation in the vapour blanket through a non-linear boundary condition. Using our mathematical  
14 model, we predict the change in the snack density as a function of time, and investigate how lift-off  
15 time depends on the different parameters of the problem.

16     **Key words.** multiphase, Stefan, asymptotic

17     **AMS subject classifications.** 80A22, 80A20, 35B40

18     **1. Introduction.** Frying is one of the oldest and most common forms of food  
19 cooking, and has multiple functions, including to sterilise, dehydrate and create prod-  
20 uct texture [1]. Generally there are two types of frying: shallow-fat frying and deep-fat  
21 frying. Here we focus on deep-fat frying in which the food product being cooked is  
22 fully immersed in the oil. During deep-fat frying, some food products undergo density  
23 changes that cause them to rise within the oil bath. This process can be exploited  
24 in food manufacturing, either as a way of determining the stage of cooking, or as a  
25 mechanism to collect the food from the hot oil. For example, in the production of  
26 potato snacks, uncooked snacks are submerged in hot oil by a conveyor belt and, as  
27 the dough cooks, they become buoyant and detach. Once the snack rises from the  
28 belt it interacts with a second submerged component. Knowing the lift off duration is  
29 key to understanding when and where the snack interacts with the second submerged  
30 component. This interaction has product quality and fryer performance implications.  
31 This must happen at precisely the right moment in order to maximise product qual-  
32 ity and the productivity of the process. To ensure that the snacks robustly detach at  
33 the right time, a better quantitative understanding of the underlying mechanism is  
34 needed. In particular, there are two major contributions to buoyancy due to the gen-  
35 eration of steam, which either escapes from the snack causing a reduction in density,  
36 or becomes trapped underneath the snack in a vapour blanket.

37     Several different mathematical modelling approaches can be found within the food  
38 frying literature. For a comprehensive summary of all relevant types of models, see

---

\*Submitted to the editors DATE. All authors contributed equally to this work. This paper has been posted as a preprint on arXiv.

<sup>†</sup>Mathematical Institute, University of Oxford, Andrew Wiles Building, Radcliffe Observatory Quarter, Woodstock Road, Oxford OX2 6GG, United Kingdom

<sup>‡</sup>LadHyX, UMR CNRS 7646, Ecole polytechnique, 91128 Palaiseau, France. Department of Earth Sciences, University of Cambridge, Bullard Laboratories, Madingley Road, Cambridge CB3 0EZ, UK

<sup>§</sup> PepsiCo International, 4 Leycroft Road, Leicester LE4 1ET, United Kingdom

<sup>¶</sup>School of Computing and Engineering, University of Huddersfield, Queensgate, Huddersfield HD1 3DH, United Kingdom. MACSI, Department of Mathematics and Statistics, University of Limerick, Limerick, Ireland. w.lee@hud.ac.uk

39 [13]. Many of these emphasise transport mechanisms of gases and liquids in porous  
40 media [13, 14, 20, 6, 8]. A commonly used modelling approach is the *crust-core* model,  
41 in which there are two regions: a dry *crust* where the water has evaporated, and a  
42 wet *core*. In the crust-core approach, mass and energy equations are used to describe  
43 the heat and flow in each region, and a moving boundary tracks the evaporation front  
44 at the crust-core interface. One major concern in the deep-fat frying literature is  
45 oil uptake into the snack, and several experiments have been gathered regarding this  
46 issue [15, 21, 16, 5, 10]. However, most of these models focus on the oil absorption  
47 post-frying, since this is when most of the oil (approximately 80%) enters the snack  
48 [14, 20]. Another important objective of many of these studies is to predict quality  
49 changes (puffiness, shrinkage, etc) in the snacks as they fry [10, 13, 20]. Some models  
50 also account for the decrease in the temperature of the oil due to moisture loss from  
51 the chip [13, 6].

52 A dominant feature of the frying process is the evaporation of the water, which can  
53 be observed both from bubbles rising to the surface, and in a vapour layer surrounding  
54 the snack. Despite the formation of a vapour blanket being mentioned in several  
55 papers (see for instance [8] where it is stated that the bubbles impede oil inflow  
56 through the bottom boundary) this process has not been described in mathematical  
57 terms before within the deep-fat frying literature. In other contexts, film boiling has  
58 been studied and expressions for the vapour layer thickness have been derived, as well  
59 as bubble generation and release frequencies [7, 4]. However, none of the above studies  
60 address the density changes undergone due to the formation of the vapour blanket,  
61 and lift-off is not investigated at all. Furthermore, the effect of the vapour layer,  
62 which is a poor conductor, on the heat transfer in the snack is also not discussed.

63 In this study, we focus on predicting when a snack becomes buoyant, which hap-  
64 pens within a few seconds of being introduced into the fryer. Thus, we do not consider  
65 structural changes, which occur later on in the frying process, nor do we consider  
66 oil-uptake, which primarily occurs post-frying. We follow the crust-core modelling  
67 approach, and we introduce the novel detail of the formation of a vapour layer under  
68 the snack. We show that the timescales associated with evaporation indicate that the  
69 formation of the vapour blanket is the dominant mechanism for lift-off. We model  
70 the growth of the vapour blanket by coupling a thin film equation to the moving-  
71 boundary problem in the snack. We show that the insulating features of the vapour  
72 blanket play an important role in the dynamics of the evaporation fronts. Whilst all  
73 of the models in the above literature are solved numerically by either finite differences  
74 or finite volumes, here we combine both numerical and analytical results and compare  
75 them together. In particular, we derive closed form solutions for the long-time behav-  
76 iour of the evaporation fronts and the shape of the vapour blanket, which are useful  
77 for the manufacturing process. Furthermore, we show that lift-off times are crucially  
78 dependent on the heat transfer properties of the snack.

79 The remainder of this paper is organised as follows. In section 2 we introduce the  
80 non-dimensional mathematical model for the thermal and flow problems within the  
81 snack and vapour blanket. By exploiting the small size of some dimensionless groups,  
82 the problem simplifies to solving an energy conservation equation for each region and  
83 a thin-film equation for the vapour blanket. A formula that relates the density of the  
84 snack to the vapour blanket thickness and the position of the evaporation fronts is also  
85 given. We first solve our model numerically in section 3 using the enthalpy method,  
86 and we are able to identify several regimes in the frying process: a heating period, the  
87 formation of the vapour blanket, and a regime where the blanket volume is constant.  
88 Motivated by these numerical results, and considering that the Stefan number of the

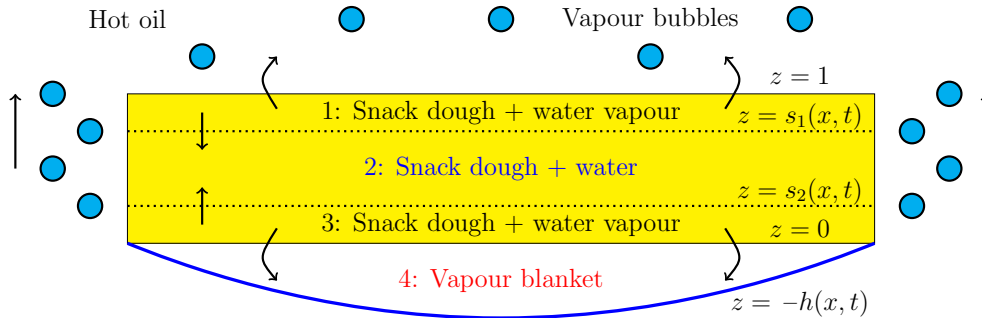


Fig. 1. Schematic diagram of the different regions in the snack.

89 problem is large, in section 4 we investigate a further simplification to the model,  
 90 called the quasi-steady limit. In this limit, where the only time-dependence of the  
 91 system originates from the motion of the evaporation fronts, we obtain analytical  
 92 solutions that agree well with the numerical results, and provide insight to the frying  
 93 behaviour. We discuss our key findings and their relevance to the snack frying process  
 94 in section 5.

95 **2. A Multiphase model for snack frying.** In Figure 1, we illustrate the  
 96 scenario considered. We focus on the two-dimensional case, as shown in the diagram,  
 97 but we keep the formulation of our mathematical model in three dimensions to be as  
 98 general as possible. We propose that the snack is divided into four regions, containing  
 99 different combinations of dough, water and water vapour. Initially, we assume the  
 100 dough to be entirely composed of a liquid (water) and solid phase (potato), which is  
 101 defined as region 2 in our diagram. When the snack is introduced into the fryer, the  
 102 water heats up and begins to evaporate, starting from the exterior. This creates two  
 103 outer layers containing water vapour and solid, which we denote regions 1 and 3. As  
 104 the water evaporates from the upper evaporation front, it is bubbled away into the  
 105 surrounding oil. By contrast, water evaporating from the lower front forms a vapour  
 106 layer beneath the snack, which we denote region 4.

107 In this section, we present a non-dimensional mathematical model for the frying  
 108 of a long thin snack, which consists of energy, mass and momentum conservation  
 109 equations for each of the different regions of the snack. We simplify these equations  
 110 by exploiting small parameters in the system. For predicting lift-off time, we introduce  
 111 a relation between the density of the snack, the size of the vapour blanket and the  
 112 position of the evaporation fronts.

113 **2.1. Mathematical model.** First, we present the governing equations for each  
 114 of the regions in Figure 1. We keep all the equations in non-dimensional form for  
 115 convenience, but later we provide further discussion on the derivation, including a  
 116 list of how each non-dimensional parameter is defined. As illustrated in the diagram,  
 117 the domain is long and thin with aspect ratio  $\epsilon = H=L^{-1}$  (where  $H$  and  $L$  are  
 118 the height and length of the snack). We model regions 1 and 3 using an advection-  
 119 diffusion equation for the temperature (due to energy conservation), and Darcy's law

120 for the fluid flow,

$$121 \quad (2.1) \quad \frac{1}{\text{St}} \frac{\partial T_i}{\partial t} + \text{Pe} \, w_i \frac{\partial T_i}{\partial z} + {}^2 \mathbf{u}_i \cdot \nabla_{xy} T_i = \frac{\partial^2 T_i}{\partial z^2} + {}^2 r_{xy}^2 T_i; \quad i = 1; 3;$$

$$122 \quad (2.2) \quad \mathbf{u}_i = -\nabla P_i; \quad i = 1; 3;$$

$$123 \quad (2.3) \quad 0 = \frac{\partial^2 P_i}{\partial z^2} + {}^2 r_{xy}^2 P_i; \quad i = 1; 3;$$

125 where  $T_i(\mathbf{x}_i; t)$  is the temperature,  $\mathbf{u}_i(\mathbf{x}_i; t) = (u_i; v_i; w_i)$  is the velocity of the fluid,  
 126 and  $P_i(\mathbf{x}_i; t)$  is the pressure. Subscripts are used to denote the different regions and  
 127  $\nabla_{xy} = (\frac{\partial}{\partial x}; \frac{\partial}{\partial y}; 0)$  is the gradient in the  $x$ - $y$  plane. Our dimensionless parameters are  
 128 the Péclet number  $\text{Pe}$ , and the Stefan number  $\text{St}$ , and their definitions can be found  
 129 in Table 1. We assume that the flow in the core region 2 of the snack is negligible,  
 130 and so there is no need for any mass or momentum equations. The heat equation in  
 131 this region is

$$132 \quad (2.4) \quad \frac{C}{\text{St}} \frac{\partial T_2}{\partial t} = K_2 \left( \frac{\partial^2 T_2}{\partial z^2} + {}^2 r_{xy}^2 T_2 \right);$$

134 where  $K_2$  and  $C$  are the ratios of thermal conductivities and volumetric heat capacities  
 135 between regions 2 and 1. In region 4, we have an advection-diffusion equation for the  
 136 temperature and the Navier-Stokes equations for the fluid flow,

$$(2.5) \quad \frac{\text{Pe}}{K_4} \left( \frac{\partial T_4}{\partial t} + \mathbf{u}_4 \cdot \nabla T_4 \right) = \frac{\partial^2 T_4}{\partial z^2} + {}^2 r_{xy}^2 T_4;$$

$$138 \quad (2.6) \quad \text{Re} \left( \frac{\partial \mathbf{u}_4}{\partial t} + \mathbf{u}_4 \cdot \nabla \mathbf{u}_4 \right) = \left( \frac{\partial P_4}{\partial x}; \frac{\partial P_4}{\partial y}; \frac{\partial P_4}{\partial z} \right)^T + \frac{\partial^2 \mathbf{u}_4}{\partial z^2} + {}^2 r_{xy}^2 \mathbf{u}_4 - \frac{\text{Re}}{\text{Fr}^2} \hat{\mathbf{z}};$$

$$139 \quad (2.7) \quad \nabla \cdot \mathbf{u}_4 = 0;$$

141 where  $K_4$  is a ratio of thermal conductivities between regions 4 and 1,  $\tau$  is the ratio  
 142 of the timescale of evaporation to the timescale of evolution of the vapour blanket  
 143  $z = h$ ,  $\text{Re}$  is the Reynolds number,  $\text{Fr}$  is the Froude number, and  $\beta$  is a measure  
 144 of the relative size of the hydrostatic pressure of the oil acting on the gas in region  
 145 4 compared to the pressure drop needed to maintain the Darcy gas flux in regions 1  
 146 and 3. On the boundaries at  $z = 1$  and  $z = h$ , we have Newton's law of heating

$$147 \quad (2.8) \quad \frac{1}{N} \frac{\partial T_1}{\partial z} = T_1 - T_{\infty}; \quad z = 1;$$

$$148 \quad (2.9) \quad \frac{K_4}{N} \left( \frac{\partial T_4}{\partial z} + {}^2 r_{xy} h \nabla_{xy} T_4 \right) = T_4 - T_{\infty}; \quad z = h;$$

150 where  $N$  is the Nusselt number, measuring the ratio between heat transfer at the  
 151 boundary and heat conduction in the snack. At the boundary,  $z = h$ , we have the  
 152 kinematic and dynamic boundary conditions

$$153 \quad (2.10) \quad \frac{\partial h}{\partial t} = w_4 - \mathbf{u}_4 \cdot \nabla_{xy} h; \quad z = h;$$

$$154 \quad (2.11) \quad \mathbf{D} \cdot \mathbf{n} = \frac{P_4}{\text{Bo}} - h \frac{\partial \mathbf{n}}{\partial z}; \quad z = h;$$

156 where  $Bo$  is the Bond number,  $\kappa$  is the curvature,  $D$  is the strain rate tensor, and  $\mathbf{n}$   
 157 is the normal to the vapour blanket, given by

$$158 \quad (2.12) \quad = \frac{\kappa^2 h}{(1 + \kappa^2 h^2)^{3/2}};$$

$$159 \quad (2.13) \quad \mathbf{D} = \frac{1}{2} \left( \frac{\partial u_4}{\partial x} + \frac{\partial v_4}{\partial x} \right) \frac{\partial v_4}{\partial y} + \frac{\partial w_4}{\partial z} + \frac{\partial u_4}{\partial x} \frac{\partial v_4}{\partial y} + \frac{\partial w_4}{\partial z} \frac{\partial u_4}{\partial x} + \frac{\partial w_4}{\partial z} \frac{\partial v_4}{\partial y} \Bigg|_A;$$

$$160 \quad (2.14) \quad \mathbf{n} = \frac{1}{\sqrt{1 + \kappa^2 h^2}} \left( \frac{\partial h}{\partial x} \mathbf{e}_x + \frac{\partial h}{\partial y} \mathbf{e}_y + \mathbf{e}_z \right);$$

162 On the evaporation fronts,  $z = s_i$  for  $i = 1, 2$ , we require that the temperature matches  
 163 the evaporation temperature of water

$$164 \quad (2.15) \quad T_1 = T_2 = 0; \quad z = s_1;$$

$$165 \quad (2.16) \quad T_2 = T_3 = 0; \quad z = s_2;$$

167 We also have a Stefan condition describing the motion of the evaporation fronts. This  
 168 condition can be derived by balancing the latent energy required to vaporise water  
 169 with difference in heat flux on either side of the boundary. This gives us

$$170 \quad (2.17) \quad \dot{s}_1 = K_2 \frac{\partial T_2}{\partial z} - \frac{\partial T_1}{\partial z} + \kappa \gamma_{xy} s_1 - \kappa \gamma_{xy} (T_1 - K_2 T_2); \quad z = s_1;$$

$$171 \quad (2.18) \quad \dot{s}_2 = K_2 \frac{\partial T_2}{\partial z} - \frac{\partial T_3}{\partial z} + \kappa \gamma_{xy} s_2 - \kappa \gamma_{xy} (T_3 - K_2 T_2); \quad z = s_2;$$

173 The change in density undergone when the water vaporises creates a flow in regions  
 174 1 and 3. As discussed by [17], the equations that describe the flow generated by this  
 175 volume change are

$$176 \quad (2.19) \quad \frac{1}{R} \dot{s}_1 = W_1 + \kappa \mathbf{u}_1 \cdot \mathbf{r}_{xy} s_1; \quad z = s_1;$$

$$177 \quad (2.20) \quad \frac{1}{R} \dot{s}_2 = W_3 + \kappa \mathbf{u}_3 \cdot \mathbf{r}_{xy} s_2; \quad z = s_2;$$

179 where  $R$  is the ratio of the density of water to the density of steam. This signifies the  
 180 volume change that happens when the water is vaporised, which drives the gas flow.

181 Finally, at the interface between the snack and the vapour blanket, we have  
 182 continuity of temperature, mass, pressure, and heat flux,

$$183 \quad (2.21) \quad T_3 = T_4; \quad P_3 = \Gamma P_4; \quad K_4 \frac{\partial T_4}{\partial z} = \frac{\partial T_3}{\partial z}; \quad z = 0;$$

$$184 \quad (2.22) \quad \kappa u_3; \kappa v_3; W_3 = [u_4; v_4; W_4]; \quad z = 0;$$

186 where  $\Gamma$  is the non-dimensional permeability of the snack. The dimensionless initial  
 187 conditions are given by

$$188 \quad (2.23) \quad T_2(\mathbf{x}; t) = T^*;$$

$$189 \quad (2.24) \quad s_1(x; y; 0) = 1;$$

$$190 \quad (2.25) \quad s_2(x; y; 0) = 0;$$

$$191 \quad (2.26) \quad h(x; y; 0) = 0;$$

193 In Table 1 we list the dimensionless parameters of the system, their definitions in  
 194 terms of dimensional parameters, and their approximate values. The dimensional

Parameter	Definition	Value
St	$L_V \rho_l = (\rho_l c_{p;1}(T_o - T_e))$	8:4
C	$c_{p;2} = c_{p;1}$	2:1
"	$H=L$	1:1 $10^{-2}$
Pe	$c_{p;4}(T_o - T_e) = L_V$	5:8 $10^{-2}$
K <sub>2</sub>	$k_2 = k_1$	1:4
K <sub>4</sub>	$k_4 = k_1$	4:2 $10^{-2}$
	$\rho_l = \rho_v$	5:8 $10^2$
Re	$k_1(T_o - T_e) = (L_V \rho_v)$	9:2 $10^{-1}$
	$L_V g \rho_o H^3 = (k_1 L^2 \rho_v (T_o - T_e))$	6:5 $10^{-1}$
Γ	$= H^2$	2:0 $10^{-4}$
N	$h_c H = k_1$	1:3
T*	$(T_a - T_e) = (T_o - T_e)$	1:1
Bo	$\rho_o g L^2 =$	1:1 $10^3$
R	$\rho_l = \rho_v$	1:7 $10^3$
Fr	$(k_1(T_o - T_e) = \rho_v L_V H^2) \rho_l \overline{L=g}$	4:3

Table 1  
 Dimensionless parameters and their approximate numerical values.

194 parameters appearing in Table 1 are:  $L_V$ , the latent heat of vaporisation of water;  
 195  $\rho_l$ , the porosity of the snack;  $\rho_v$ , the permeability of the snack;  $h_c$ , the heat transfer  
 196 coefficient;  $\rho_o$ , the interfacial tension between water and oil;  $g$ , the acceleration due  
 197 to gravity;  $H$ , the height of the snack;  $L$ , the length of the snack;  $\rho_v$ , the viscosity  
 198 of water vapour;  $T_o$ ,  $T_l$ ,  $T_a$ , the temperature of the oil, the evaporation temperature  
 199 of water, and the ambient air temperature of the snack before entry into the oil;  
 200 and  $\rho_o$ ,  $\rho_l$ ,  $\rho_v$ , the density of oil, water, and vapour, respectively. Finally, we have  
 201 some compound parameters for regions 1, 2, and 3, each with a subscript denoting  
 202 the relevant region. These are:  $\rho_j$ , the compound density;  $k_j$  the compound thermal  
 203 conductivity; and  $c_{p;j}$ , the compound specific heat capacity, with  $j = 1 - 4$ . These  
 204 compound parameters have been determined by taking a volume-weighted-average of  
 205 the parameters for the individual phases (solid snack, water, vapour) in each region  
 206 (see [11] for instance). For example,  $\rho_1 = \rho_s \rho_s + \rho_v \rho_v$ , where each  $\rho_i$  represents a  
 207 mass fraction.

209 **2.2. Model simplifications.** Having calculated the non-dimensional parame-  
 210 ters in Table 1, we are motivated to consider the asymptotic limit of

$$211 \quad (2.27) \quad \text{Pe}; \rho_l; \text{Re}; \text{Bo}^{-1}; \text{Pe}=\text{K}_4; \text{Pe}=\text{K}_4; \text{Re}=\rho_l; \text{K}_2; \text{Re}=\text{Fr}^2; 1=\text{R} \neq 0:$$

212 Note that although a few of these parameter groups associated with the vapour layer  
 213 (Re, Pe/K<sub>2</sub>) are marginal in this scaling, we have also carried out a more complex  
 214 scaling in which the thicknesses of regions 3 and 4 are scaled separately. This scaling  
 215 confirms that all the dimensionless quantities listed above are small.

216 Under these limits, the only coupling between the flow and thermal problems  
 217 is through the boundary conditions (2.10), (2.11), (2.19) and (2.20). The simplified

218 governing equations for the heat problem are

$$219 \quad (2.28) \quad \frac{1}{St} \frac{\partial T_1}{\partial t} = \frac{\partial^2 T_1}{\partial Z^2}; \quad S_1 \leq Z \leq 1;$$

$$220 \quad (2.29) \quad \frac{C}{St} \frac{\partial T_2}{\partial t} = K_2 \frac{\partial^2 T_2}{\partial Z^2}; \quad S_2 \leq Z \leq S_1;$$

$$221 \quad (2.30) \quad \frac{1}{St} \frac{\partial T_3}{\partial t} = \frac{\partial^2 T_3}{\partial Z^2}; \quad 0 \leq Z \leq S_2;$$

223 The only dependence of the heat problem on the thickness of the vapour blanket  
224  $h$  is through the lower boundary condition. Hence, the complete set of boundary  
225 conditions for the heat problem are

$$226 \quad (2.31) \quad \frac{1}{N} \frac{\partial T_1}{\partial Z} = 1 - T_1; \quad Z = 1;$$

$$227 \quad (2.32) \quad T_1 = T_2 = 0; \quad Z = S_1;$$

$$228 \quad (2.33) \quad \dot{S}_1 = K_2 \frac{\partial T_2}{\partial Z} - \frac{\partial T_1}{\partial Z}; \quad Z = S_1;$$

$$229 \quad (2.34) \quad T_2 = T_3 = 0; \quad Z = S_2;$$

$$230 \quad (2.35) \quad \dot{S}_2 = K_2 \frac{\partial T_2}{\partial Z} - \frac{\partial T_3}{\partial Z}; \quad Z = S_2;$$

$$231 \quad (2.36) \quad \frac{1}{N} \frac{\partial T_3}{\partial Z} - \frac{hN}{K_4} + 1 = T_3 - 1; \quad Z = 0;$$

233 where equation (2.36) is derived by solving for  $T_4$  and inserting the solution into  
234 (2.21). Specifically,  $T_4$  is given in terms of  $T_3$  and  $h$  by

$$235 \quad (2.37) \quad T_4 = 1 + \frac{1}{N} \left[ \frac{(Z+h)N}{K_4} + 1 \right] \frac{\partial T_3}{\partial Z} \Big|_{z=0};$$

236 In order to obtain an equation for  $h$ , we need to follow a series of steps. Firstly, taking  
237 the third component of the simplified version of (2.6) together with the reduced form  
238 of (2.11) we obtain  $P_4 = h$  throughout region 4. Now,  $\mathbf{u}_4$  can be found simply by  
239 integrating the reduced form of the first two components of (2.6), as well as (2.7).  
240 Substituting this into the kinematic condition (2.10) gives

$$241 \quad (2.38) \quad -\frac{1}{3} \frac{\partial h}{\partial t} = \frac{1}{3} r_{xy} - h^3 r_{xy} h - w_4|_{z=0};$$

242 Finally, by considering the fluid problem in region 3, and using the simplified version  
243 of (2.20), we see that  $w_4|_{z=0} = \dot{S}_2$ . Thus, the governing thin-film equation for the  
244 vapour blanket becomes

$$245 \quad (2.39) \quad -\frac{1}{3} \frac{\partial h}{\partial t} = \frac{1}{3} r_{xy} - h^3 r_{xy} h + \dot{S}_2;$$

246 We would expect that at the edges of the snack,  $h$  would take some finite value and  
247 the pressure would be equivalent to the hydrostatic pressure of the oil. However, in  
248 our thin film equation (2.39) we cannot impose both these conditions, so we choose

$$249 \quad (2.40) \quad h = 0; \text{ at } \Omega_0;$$

250 as the lateral boundary condition, where  $\Omega_0$  is the cross-section of the snack at  $z = 0$ ,  
251 and  $\Omega_0$  is the boundary of  $\Omega_0$ . We note that in choosing this boundary condition,

252 we will see that the  $h$  will have to have infinite slope at the edges in order to have a  
 253 finite flux.

254 Note that whilst the vapour blanket thickness depends spatially on  $x$  and  $y$ ,  
 255  $h = h(x, y, t)$ , the temperature only depends on  $z$ , except for the boundary condition  
 256 (2.36). Hence, it is convenient to replace  $h$  in (2.36) by an average film thickness  
 257  $\bar{h} = \frac{1}{\Omega_0} \int_{\Omega_0} h dx dy$ . Making this substitution, the thermal problem is purely in terms  
 258 of  $z$ , and the vapour blanket problem is in terms of  $x$  and  $y$ . We can simplify even  
 259 further by assuming that the snack is uniform in the  $y$  direction, giving us a one-  
 260 dimensional model for the thermal problem in  $z$ , and a one-dimensional model for the  
 261 vapour blanket problem in  $x$ . This is the approach taken for the remainder of this  
 262 study.

263 **2.3. Density calculation and lift-off time.** A necessary condition for the  
 264 snack to detach from the conveyor belt is that its density is less than that of the  
 265 surrounding oil. The reduction of the density of the snack is due to two processes.  
 266 Firstly there is loss of mass as water evaporates into steam and leaves the snack.  
 267 Secondly the formation of the vapour blanket increases the volume of the snack.

268 The dimensionless density,  $\rho$ , is scaled by the density of oil,  $\rho_o$ , so that  $\rho = 1$   
 269 when the snack is neutrally buoyant. The density is given by

271 (2.41) 
$$\rho(t) = \frac{\int_0^1 \int_0^1 h dx dy}{1 + \frac{v}{o} \int_0^1 h dx} + \frac{l}{o} \rho_l (s_1 - s_2) + \frac{v}{o} \rho_v [1 - (s_1 - s_2)] + \frac{s}{o} \rho_s :$$

274 The denominator is the volume of the snack, including the volume of the bubble  
 275 given by integrating over  $h$ . The numerator is the mass of the snack broken into  
 276 contributions from the gas in the bubble, liquid water in region 2, water vapour in  
 277 regions 1 and 3 and the solid component of the snack. Therefore, the non-dimensional  
 278 lift-off time, which we denote  $t^*$ , is the first time<sup>1</sup> for which

279 (2.42) 
$$\rho(t^*) < 1:$$

280 **3. Numerical Approach.** Our first approach is to solve the problem (2.28)-  
 281 (2.30), (2.39) numerically using the enthalpy method [3, 18]. The non-dimensional  
 282 temperature,  $T$ , is related to the non-dimensional enthalpy,  $h$ , in the following way:

283 (3.1) 
$$T = \begin{cases} \frac{h - h_c}{C} : & h < h_c \\ 0 : & h_c \leq h \leq h_l \\ \frac{h - h_l}{St(h_l - h_c)} : & h > h_l \end{cases}$$

284 The enthalpy method conveniently reduces the problem to solving the single partial  
 285 differential equation

286 (3.2) 
$$\frac{\partial h}{\partial t} = \frac{\partial^2 T}{\partial z^2};$$

287 within the entire domain  $0 \leq z \leq 1$ , where  $h$  and  $T$  are related via (3.1). We  
 288 solve (2.39) and (3.2) using the method of lines with a fourth order central finite

<sup>1</sup>Note that in reality, there may be some surface tension effects holding the snack down to the solid substrate, therefore delaying lift-off time. However, since these depend on the specific surface properties of the fryer substrate, we do not study such effects here.



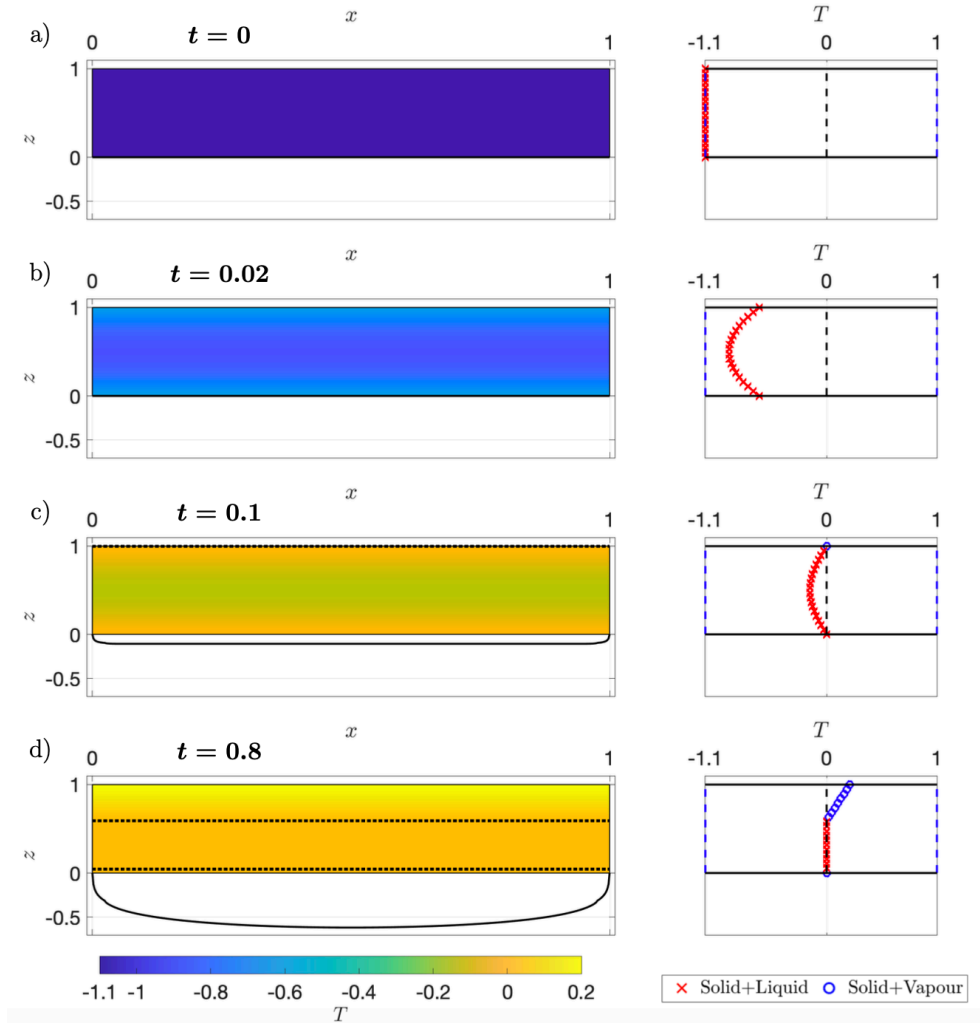


Fig. 2. (a,b,c,d) Numerical solution at  $t = 0; 0.02; 0.1; 0.8$ , showing a colour plot of the temperature in the snack, a corresponding line plot of the temperature, and the  $l_m$  thickness beneath the snack.

289 difference scheme in space and a fourth order explicit Runge-Kutta scheme in time,  
 290 where at each time step we update  $T$  using the relation (3.1). It is possible to achieve  
 291 even greater accuracy using other more detailed schemes, such as adaptive time-  
 292 stepping and spectral methods, but we find that our current approach is well within  
 293 the convergence regime and is sufficiently accurate for the purposes of this study.

294 We plot the solution in Figures 2 and 3, illustrating the evolution of the temper-  
 295 ature, the vapour blanket, and the resultant snack density. We identify several  
 296 clear regimes in the frying process, which we indicate in the density plot in Figure  
 297 3a). Initially the snack is plunged into the oil at room temperature, and so the first  
 298 regime consists of a heating period, bringing the temperature within the snack to  
 299 the evaporation temperature. During this *heat diffusion* regime, the snack is entirely

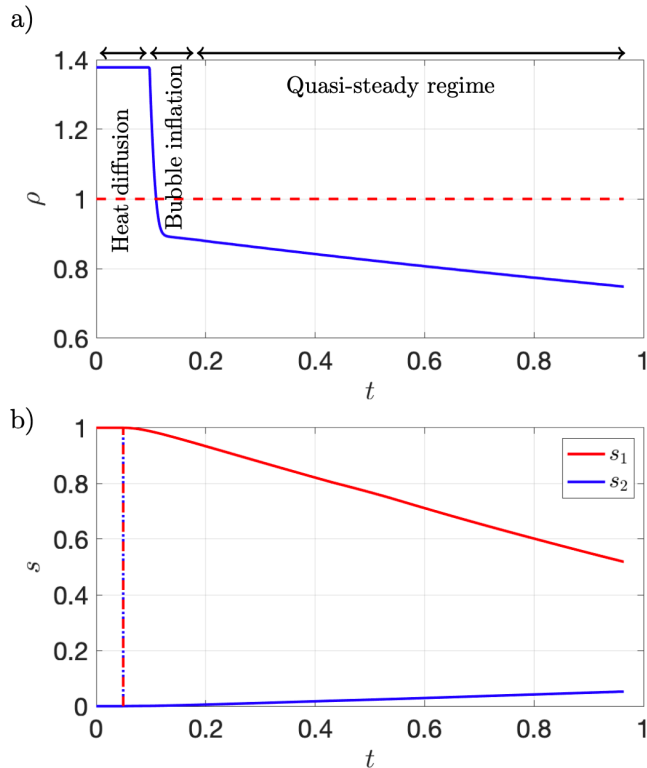


Fig. 3. (a) Numerical solution for the density evolution over time, indicating the critical density for lift-off  $\rho_c = 1$ . (b) Evolution of the evaporation fronts  $s_1$  and  $s_2$ .

300 composed of liquid and solid (region 2). Once the temperature is near the boiling  
301 point everywhere, and equal to the boiling temperature at the edges of the snack, the  
302 latent heat begins to be removed. As the latent heat is removed from the edges of  
303 the snack, two evaporation fronts recede into the interior of the snack, bubbling away  
304 vapour through the top and bottom. This is the second regime of the process, during  
305 which the vapour blanket is formed, and inflates very rapidly, causing a sudden drop  
306 in density. Hence, this is denoted the *bubble inflation* regime. However, the vapour  
307 blanket quickly reaches a steady state, bringing us to the third and final regime of  
308 the process. During this regime, even though the blanket thickness is approximately  
309 constant, the evaporation fronts continue to move inwards, and so we denote this the  
310 *quasi-steady regime*. In particular, the fact that the blanket remains at near-constant  
311 volume can only be explained by a constant growth rate of the evaporation front  $s_2$   
312 in (2.39), and this is in accordance with our numerical observations in Figure 3b).  
313 Furthermore, the temperature within each region is approximately linear with  $z$ , as  
314 can be seen in Figure 2d). This piecewise linear temperature profile, which is char-  
315 acteristic of the quasi-steady limit [3, 12, 2], is due to the large Stefan number in  
316 (2.28)-(2.30). Later in section 4 we will use our numerical observations from Figure  
317 2d) to motivate an asymptotic treatment of the quasi-steady behaviour by taking the  
318 limit of large Stefan number. We also note that, as mentioned at the end of Section  
319 2.2, the slope of the blanket at the edges of the snack is infinite, which is most visible

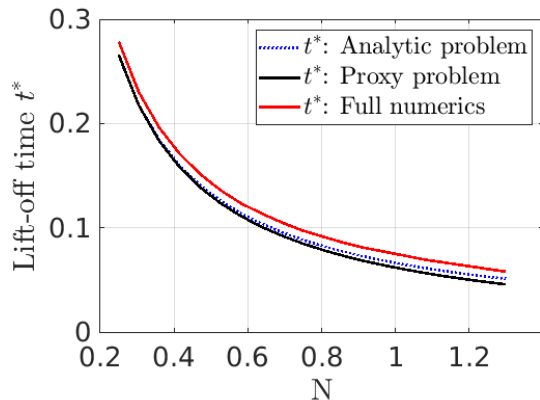


Fig. 4. Variation of the non-dimensional lift-off time with Nusselt number  $N$ , showing the analytic times, the approximate times calculated by solving the proxy heat diffusion problem until first evaporation, and the precise times calculated by solving the full numerical problem until  $(t^*) < 1$ .

320 in Figure 2d). Thus, we have used a refined spatial grid in the numerical solution.

321 The lift-off time of the snack is taken as the time at which the density falls below  
 322 the oil density (2.42). For the parameters used here, this corresponds to a time of  
 323  $t = 0.1$ , or in dimensional terms, 1 second, which is in agreement with observations  
 324 in the frying industry. A key result from our model is that the lift-off time is largely  
 325 controlled by the inflation of the vapour blanket. In fact, since the bubble inflation  
 326 is so rapid and causes such a large relative change in volume, the time for lift-off is  
 327 only marginally larger than the time needed for first evaporation (see Figure 3a)).  
 328 Hence, as a proxy for the lift-off time, one can simply solve the initial heat diffusion  
 329 problem (first regime) and find the time at which the latent heat is first removed from  
 330 the bottom boundary  $z = 0$ . Such an approach reduces the computational cost and  
 331 technical complexity of the problem since it avoids having to resolve the growth of the  
 332 vapour blanket. Following this proxy approach, the key parameter that determines  
 333 the lift-off time is the Nusselt number  $N$ , which is a measure of the ratio between heat  
 334 transfer at the boundary and heat conduction in the snack. We can further simplify  
 335 this proxy problem in order to derive an analytic formula for  $t^*$  as a function of  $N$ .  
 336 We do this by integrating the heat equation from the bottom to the top of the crisp,  
 337 substituting in the Newton heating boundary conditions, then assuming the average  
 338 temperature in the crisp and the temperature at the top and bottom of the crisp are  
 339 all approximately equal. Doing this we recover an ODE for the temperature of the  
 340 crisp, which we can solve to recover

$$341 \quad (3.3) \quad t^*(N) = \frac{C}{2NStK_2} \log(1 - T^*)$$

343 In the literature the Nusselt number for snacks varies between 0.3 and 1.3. Therefore,  
 344 in Figure 4 we plot the variation of approximate lift-off time with Nusselt number  
 345 calculated using the analytic formula, the proxy approach, and the full numerical  
 346 problem for  $t^*$  such that  $(t^*) < 1$ . The lift-off time is a monotone decreasing function  
 347 of  $N$ , as expected. In dimensional terms lift-off occurs for times between 0.5 and 2.6  
 348 seconds.

349 As a further motivation for our vapour blanket model, suppose instead we were

350 to ignore the vapour blanket, and just solve the classic Stefan problem with Newton  
 351 heating boundary conditions (i.e.  $h = 0$ ). In this case, we skip the second regime  
 352 since there is no bubble inflation, and simply move from a heat diffusion regime to  
 353 a quasi-steady regime. From Figure 3a) we see that the density decay in the quasi-  
 354 steady regime is much slower than that caused by bubble inflation. This results in a  
 355 lift-off time closer to  $t = 1$ , which in dimensional terms corresponds to more than 10  
 356 seconds, and this is a factor of ten larger than experimental observations. Hence, this  
 357 serves as a good indication that our vapour blanket model is accurate, and provides  
 358 the essential ingredients to predict the lift-off time during frying.

359 Motivated by the above simulations, we now consider a further limiting case of  
 360 the mathematical model called the quasi-steady limit. In this limit, we can further  
 361 simplify the governing equations and find some analytical results that provide useful  
 362 insight to the problem.

363 **4. Quasi-steady limit.** The quasi-steady limit corresponds to when the thermal  
 364 problem (2.28)-(2.30) becomes independent of time except through the motion of the  
 365 evaporation fronts. This limit, which is typical in such phase change problems, is a  
 366 result of the fact that the Stefan number is large [3, 12, 2]. In our case,  $St = O(10)$ ,  
 367 which, though not large in the absolute sense, is large enough for the purposes of  
 368 our asymptotic analysis, as the numerical results suggest. It is often the case that  
 369 an asymptotic result valid when a certain parameter is large is also valid beyond this  
 370 range. To study this limit, we restrict our attention to the second and third regimes  
 371 of the above simulations. That is to say, we replace the initial conditions at room  
 372 temperature (2.23) that we used previously with initial conditions at the evaporation  
 373 temperature  $T(t=0) = 0$ . As before, we restrict our attention to the case where the  
 374 evaporation fronts move uniformly, such that  $s_1, s_2$  and  $T_1-T_3$  are independent of  $x$   
 375 and  $y$ . Hence, the temperature in each region is given by

376 (4.1) 
$$T_i = A_i(t)z + B_i(t);$$

378 for some functions  $A_i; B_i$ , for  $i = 1-4$ . The thermal profiles (4.1) are consistent with  
 379 our numerical observations in Figure 2d), where the temperature is approximately  
 380 linear within each region.

381 Applying the boundary conditions (2.31)-(2.36), we obtain

382 (4.2) 
$$T_1 = \frac{z - s_1}{1 + 1=N} \frac{s_1}{s_1};$$

383 (4.3) 
$$T_2 = 0;$$

384 (4.4) 
$$T_3 = \frac{s_2 - z}{1=N + \bar{h}=K_4 + s_2};$$

385 (4.5) 
$$\dot{s}_1 = \frac{1}{1 + 1=N} \frac{1}{s_1};$$

386 (4.6) 
$$\dot{s}_2 = \frac{1}{1=N + \bar{h}=K_4 + s_2};$$

387

388 The last equation (4.6) contains the spatial average of the vapour blanket thickness,  
 389  $\bar{h} = \int_0^1 h dx$ , which is found by solving the thin-film equation

390 (4.7) 
$$\frac{1}{3} \frac{\partial h}{\partial t} = \frac{\partial}{\partial x} \left( h^3 \frac{\partial h}{\partial x} \right) + \frac{1}{1=N + \bar{h}=K_4 + s_2};$$

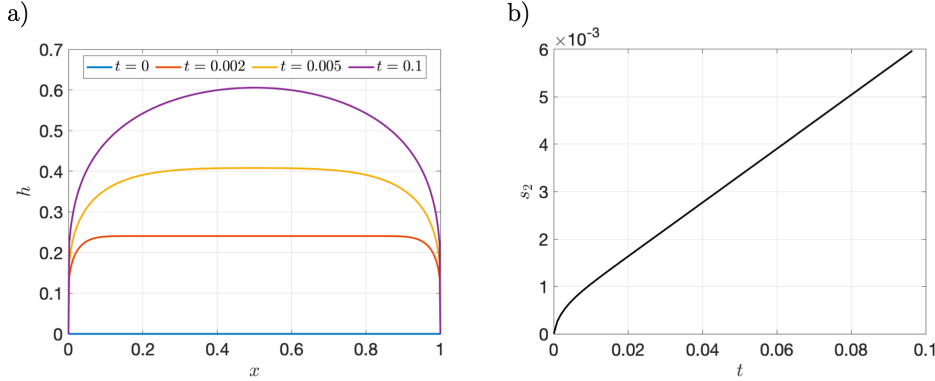


Fig. 5. Solution to the quasi-steady approximation. (a) Evolution of the thin film  $h$  at various times. (b) Evolution of the lower evaporation front  $s_2(t)$ .

391 together with the boundary conditions  $h = 0$  at  $x = 0;1$  from (2.40). We again note  
 392 that we expect the slope of  $h$  to be infinite at the edges to be consistent with the  
 393 requirement for a finite non-zero flux. We can solve (4.5) immediately, finding

394 (4.8) 
$$s_1 = \frac{1}{N} \sqrt{1 + N^2 t} :$$

395 The form of (4.8) reveals the classic  $t^{1/2}$  similarity behaviour that is discussed for  
 396 Stefan problems in the literature [19, 9]. The remaining unknowns  $h$  and  $s_2$  are  
 397 found by solving the coupled system (4.6)-(4.7). In Figure 5 we display the numerical  
 398 solution to this system, calculated using the method of lines, as before. We see a fast  
 399 early-time growth of the evaporation front  $s_2$ , causing a rapid inflation of the bubble  
 400 over a timescale of around  $t = 0.01$ . After this inflation period, the growth rate of  $s_2$   
 401 is almost constant, and consequently the bubble shape reaches a steady state, which  
 402 is consistent with Figures 2,3.

403 To understand the apparent steady state, let us consider the evolution equation  
 404 for the lower evaporation front (4.6). It is not immediately obvious that (4.6) yields  
 405 a constant growth rate solution. However, the non-dimensional conductivity ratio is  
 406 very small  $K_4 = 0.04$ , and  $s_2$  in Figure 5 is also very small, suggesting that perhaps  
 407 the variables  $s_2$  and  $h$  ought to be rescaled by  $K_4$  appropriately. Since, for the steady  
 408 state solution, we expect  $h$  to be independent of time but dependent on space, and  
 409 we expect the evaporation front to move at a linear growth rate, we seek a rescaling  
 410 of the form

411 (4.9) 
$$s_2 = K_4^c(a + bt) + O(K_4^{2c});$$

412 (4.10) 
$$h = K_4^d H(x) + O(K_4^{2d});$$

414 for some unknown coefficients  $a; b; c; d > 0$ . By inserting the above into (4.6)-(4.7),  
 415 we can see that a steady state is only possible (to leading order) if we choose

416 (4.11) 
$$d - 1 + c = 0;$$

417 (4.12) 
$$4d = c;$$

419 which has solution  $c = 4=5$  and  $d = 1=5$ . Taking the limit of small  $K_4$ , the resulting  
 420 system of equations is

421 (4.13) 
$$b = \frac{1}{\bar{H}};$$

422 (4.14) 
$$\frac{1}{3} H^3 H_x + \frac{1}{\bar{H}} = 0;$$
  
 423

424 where  $\bar{H} = \int_0^1 H dx$  is the scaled average film thickness, which is a constant in the  
 425 steady state. We can solve (4.14) to give  $H$  in terms of its average value

426 (4.15) 
$$H = \frac{6x(1-x)^{1=4}}{\bar{H}};$$

427 where we notice that the slope of  $H$  is indeed infinite at  $x = 0;1$ .  $\bar{H}$  is found by  
 428 integrating (4.15), which gives

429 (4.16) 
$$\bar{H} = \frac{\Gamma(5=4)}{\Gamma(3=4)} \frac{8}{27}^{1=4 \# 4=5};$$

430 where  $\Gamma$  is the Euler Gamma function. Note that the above is only valid for times  
 431 much smaller than  $t = K_4^{-4=5} = 13$ . However, the snack frying process all takes place  
 432 within  $0 < t < 1$ , so this is acceptable. Note also that the linear behaviour of  $S_2$  with  
 433 respect to time is different from the square root behaviour of  $S_1$  observed in (4.8).  
 434 Hence, the vapour blanket completely changes evaporation at the lower boundary.

435 In Figure 6 we display a comparison of the results from the quasi-steady limit,  
 436 including the steady state, to the original numerical solution from Figures 2,3. For  
 437 the comparison, we look at the long-time evolution of the film thickness, the density,  
 438 the evaporation fronts and the temperature within the snack. We see that in all  
 439 cases there is close agreement between the numerical solution to the full problem,  
 440 the quasi-steady solution and the steady state. There is a slight discrepancy (  
 441 5%) for the steady state solution to the thin film, and this can be explained by the  
 442 asymptotic approximation (4.10) and the fact that the Stefan number is not very  
 443 large. Indeed, the correction to the leading-order approximation in  $1=St$  is  $O(1=St)$ ,  
 444 which is comparable to the magnitude of the discrepancy we see between the numerical  
 445 solution to the full problem and the quasi-steady result. This discrepancy could be  
 446 mitigated by going to higher order terms in the asymptotic expansions.

447 There is also a slight disagreement (1%) between the early-time density pre-  
 448 dictions of the numerical solution to the full problem and the quasi-steady solution.  
 449 This can be explained by the way in which we calculate the speed of the lower evap-  
 450 oration front  $S_2$ , which largely controls the density at early times via the inflation of  
 451 the vapour blanket. In the quasi-steady approximation we calculate the evaporation  
 452 front  $S_2$  using a numerical discretisation scheme in time to solve (4.6), with time step  
 453  $\Delta t = 4 \times 10^{-8}$ , providing very smooth results. On the other hand, in the numerical  
 454 solution to the full problem, since we calculate the temperature using the enthalpy  
 455 method, which does not require tracking the position of the fronts, the evaporation  
 456 front is calculated by finding the grid point that separates liquid and gas phases.  
 457 Since the grid spacing is finite, this leads to non-smooth step changes in  $S_2$  and spikes  
 458 in the time-derivative of  $S_2$ , which we have attempted to smooth using a damping  
 459 method. Nevertheless, even with a time step  $\Delta t = 4 \times 10^{-8}$ , this produces inevitable

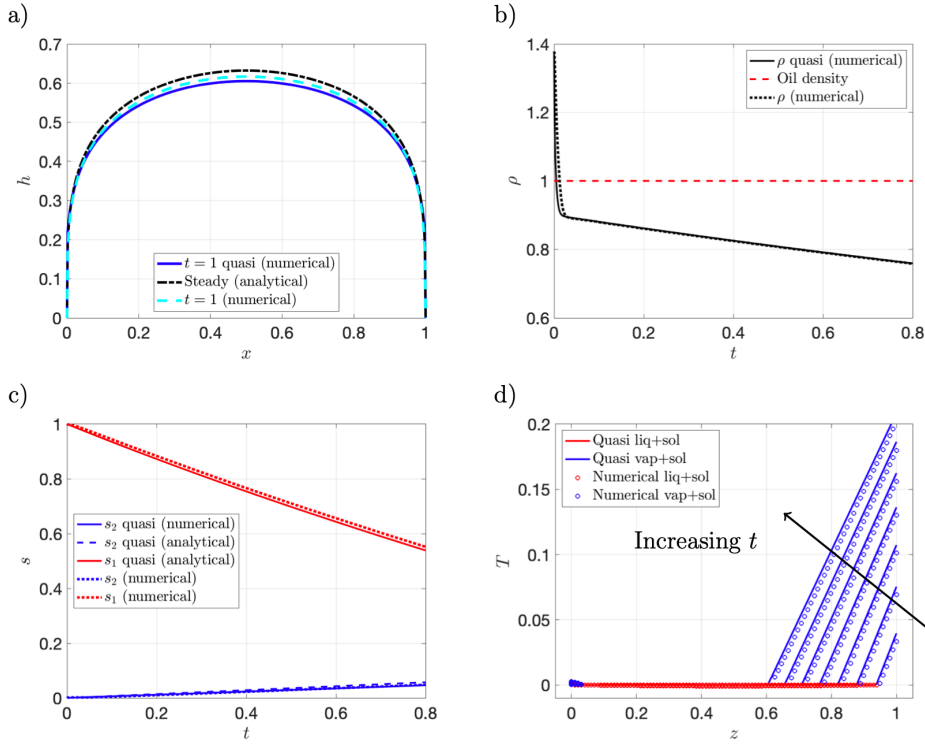


Fig. 6. Long time results from the quasi-steady approximation. (a) Evolution of the thin  $h$  at various times, compared to the analytical solution for the steady state. (b) Density  $\rho(t)$  as a function of time, indicating the lift-off density  $\rho = 1$ . (c) Evolution of the lower Stefan boundary  $s_2(t)$ , compared to the analytical solution for the steady state  $s_2 = K_4^{1/5} = \bar{H}$ . (d) Temperature profiles  $T(z; t)$  at different times between  $t = 0$  and  $t = 1$ , indicating liquid and vapour regions.

460 error associated with the inflation of the vapour blanket, and this is reflected in the  
 461 slight disagreement for the density prediction at early times.

462 Closer agreement can be attained with an even smaller spatial discretisation,  
 463 but due to the explicit discretisation method, this results in lengthy computation  
 464 times. Hence, interestingly the quasi-steady solution, though it only applies to an  
 465 asymptotic limit, is generally more accurate than the numerical solution to the full  
 466 problem. Since the critical time of interest is the lift-off time, which still shows close  
 467 agreement between these two approaches, we do not consider this discrepancy to be  
 468 very important.

469 Finally, in Figure 6 c,d) we display a comparison of the predictions of the evapora-  
 470 tion fronts and the temperature. On a macroscopic level, there is very close agreement,  
 471 and in particular the steady state solution performs remarkably well. After a time  
 472 of  $t = 1$ , or 10 seconds in dimensional terms, nearly half the liquid in the snack has  
 473 evaporated and the density has dropped by a factor of around 2. The overall thickness  
 474 of the vapour blanket is nearly equal to the total width of the snack, which is also  
 475 consistent with experimental observations.

476 **5. Conclusions.** We considered a mathematical model of potato snack frying  
477 to estimate the time at which the snack becomes less dense than the surrounding  
478 oil and begins to float, also known as the lift-off time. To that end, we modelled  
479 the frying process as a Stefan problem with two propagating evaporation fronts at  
480 which the liquid in the dough evaporates, thereby decreasing the density of the snack.  
481 In addition, a key feature in our model is the presence of a vapour blanket that  
482 forms underneath the snack as liquid evaporates. The moving evaporation fronts  
483 and the vapour blanket were assumed to be the two main mechanisms for density  
484 reduction of the snack and, therefore, its eventual lift-off. Numerical results of the  
485 full system, using the enthalpy method, revealed that both of these mechanisms were  
486 indeed essential to predict a physically realistic lift-off time of the order of one second.

487 Two simplifications to the model were presented which gave useful insights into  
488 the frying process and reduced the computation time. Firstly, since the inflation of  
489 the vapour blanket causes a significant decrease in the snack density over a very short  
490 timescale, we demonstrated that the lift-off time could be well approximated by the  
491 time for first evaporation instead. This calculation is computationally cheaper and less  
492 technically complex since it avoids modelling the vapour blanket dynamics. Secondly,  
493 due to the large Stefan number we considered a simplified quasi-steady model to  
494 describe the late-time dynamics. Both numerical and analytical solutions to this  
495 simplified model were presented, showing close agreement with solutions to the full  
496 system. This quasi-steady approximation not only further reduces the computational  
497 cost, but also provides key insights, such as the steady-state shape of the vapour  
498 blanket at late times.

499 One of the key dimensionless parameters that emerged as part of our analysis  
500 was the Nusselt number  $N$ , which is the ratio between heat transfer at the snack  
501 boundary and heat conduction in the snack interior. We investigated how changing  
502 this parameter affects the lift-off time of the snack, which is important for snack  
503 manufacturers since changing the dough, for example, can alter the Nusselt number  
504 via the material properties. Hence, knowledge of the dependence of the lift-off time  
505 on  $N$  is useful in determining optimal cooking strategies.

506 To further improve the prediction of lift-off time, other forces on the snack could  
507 be considered. These could include interfacial tension between the snack and its  
508 substrate (the conveyor belt) as well as the peeling energy required to overcome the  
509 dough elasticity. As a result, the orientation of the snack on the belt and indeed the  
510 belt design and material could have a further impact on the lift-off time of the snack.

511 **Acknowledgments.** The authors would like to acknowledge the 138th European  
512 Study Group with Industry which was held in Bath, 16-20 July 2018, and jointly  
513 hosted by the University of Bath and University of Bristol. The authors are also  
514 thankful to all the participants of the ESGI project for useful discussions: Peter Bad-  
515 doo (University of Cambridge, UK), Sean Bohun (University of Ontario, Canada),  
516 Stephen Cowley (University of Oxford, UK), Helen Fletcher (University of Oxford,  
517 UK), Harry Reynolds (University of Oxford, UK), and Chris Sear (University of  
518 Cambridge, UK). Special thanks to PepsiCo for proposing the problem and fund-  
519 ing the work throughout the ESGI, and for their collaboration during and after the  
520 study group was held. The views expressed in this article are those of the authors  
521 and do not necessarily reflect the position or policy of PepsiCo, Inc. Kris Kiradjiev,  
522 Thomas Babb and Raquel Gonzalez-Farina would also like to acknowledge the sup-  
523 port of EPSRC Center for Doctoral Training in Industrially Focused Mathematical  
524 Modelling (EP/L015803/1).



- 526 [1] S. Bakalis, K. Knoerzer, and P. J. Fryer, editors. *Modeling Food Processing Operations*. Wood-  
527 head Publishing, 2015.
- 528 [2] SI Barry and J Caunce. Exact and numerical solutions to a stefan problem with two moving  
529 boundaries. *Applied Mathematical Modelling*, 32(1):83–98, 2008.
- 530 [3] GP Benham, K Hildal, CP Please, and RA Van Gorder. Solidification of silicon in a one-  
531 dimensional slab and a two-dimensional wedge. *International Journal of Heat and Mass*  
532 *Transfer*, 98:530–540, 2016.
- 533 [4] SJ Board and RW Hall. Recent advances in understanding large scale vapour explosions. In  
534 *Third Specialist Meeting on Sodium Fuel Interactions in Fast Reactors, Tokyo, March,*  
535 *1976.*
- 536 [5] P Bouchon, P Hollins, M Pearson, DL Pyle, and MJ Tobin. Oil distribution in fried potatoes  
537 monitored by infrared microspectroscopy. *Journal of Food Science*, 66(7):918–923, 2001.
- 538 [6] Y Chen and RG Moreira. Modelling of a batch deep-fat frying process for tortilla chips. *Food*  
539 *and Bioproducts Processing*, 75(3):181–190, 1997.
- 540 [7] VK Dhir. Viscous hydrodynamic instability theory of the peak and minimum pool boiling heat  
541 fluxes. In *College of Engineering, University of Kentucky, UKY BU100*, 1972.
- 542 [8] A Halder, A Dhall, and AK Datta. An improved, easily implementable, porous media based  
543 model for deep-fat frying: Part i: Model development and input parameters. *Food and*  
544 *Bioproducts Processing*, 85(3):209–219, 2007.
- 545 [9] SD Howison. Similarity solutions to the stefan problem and the binary alloy problem. *IMA*  
546 *Journal of Applied Mathematics*, 40(3):147–161, 1988.
- 547 [10] ML Kawas and RG Moreira. Characterization of product quality attributes of tortilla chips  
548 during the frying process. *Journal of Food Engineering*, 47(2):97–107, 2001.
- 549 [11] KB Kiradjiev, SA Halvorsen, RA Van Gorder, and SD Howison. Maxwell-type models for the  
550 effective thermal conductivity of a porous material with radiative transfer in the voids.  
551 *International Journal of Thermal Sciences*, 145, 2019.
- 552 [12] B Louro and JF Rodrigues. Remarks on the quasi-steady one phase stefan problem. *Proceedings*  
553 *of the Royal Society of Edinburgh Section A: Mathematics*, 102(3-4):263–275, 1986.
- 554 [13] RG Moreira. Deep-fat frying. In *WIT Transactions on State of the Art in Science and Engi-*  
555 *neering*, volume 13. WIT press, 2007.
- 556 [14] RG Moreira and MA Barrufet. A new approach to describe oil absorption in fried foods: a  
557 simulation study. *Journal of Food Engineering*, 35(1):1–22, 1998.
- 558 [15] RG Moreira, X Sun, and Y Chen. Factors affecting oil uptake in tortilla chips in deep-fat frying.  
559 *Journal of Food Engineering*, 31(4):485–498, 1997.
- 560 [16] PC Moyano and F Pedreschi. Kinetics of oil uptake during frying of potato slices: Effect of  
561 pre-treatments. *LWT-Food Science and Technology*, 39(3):285–291, 2006.
- 562 [17] TG Myers, MG Hennessy, and M Calvo-Schwarzwalder. The stefan problem with variable ther-  
563 mophysical properties and phase change temperature. *arXiv preprint arXiv:1904.05698*,  
564 2019.
- 565 [18] V Voller and M Cross. Accurate solutions of moving boundary problems using the enthalpy  
566 method. *International Journal of Heat and Mass Transfer*, 24(3):545–556, 1981.
- 567 [19] MG Worster, GK Batchelor, and HK Moffatt. Solidification of fluids. *Perspectives in uid*  
568 *dynamics*, 742:393–446, 2000.
- 569 [20] R Yamsaengsung and RG Moreira. Modeling the transport phenomena and structural changes  
570 during deep fat frying: Part i: Model development. *Journal of Food Engineering*, 53(1):1–  
571 10, 2002.
- 572 [21] AM Ziaifar, N Achir, F Courtois, I Trezzani, and G Trystram. Review of mechanisms, condi-  
573 tions, and factors involved in the oil uptake phenomenon during the deep-fat frying process.  
574 *International Journal of Food Science & Technology*, 43(8):1410–1423, 2008.